Biomedical Microdevices (2020) 22:17
https://doi.org/10.1007/s10544-020-0472-z

Screen-printed electrochemical biosensor based on a ternary Co@MoS_2/rGO functionalized electrode for high-performance non-enzymatic glucose sensing

Xiao Li[1] · Man Zhang[1] · Yujie Hu[1] · Jian Xu[1] · Dongke Sun[1] · Tao Hu[1] · Zhonghua Ni[1]

Abstract
In this study, cobalt oxides functionalized MoS_2/reduced graphene oxide was synthesized via a facile one-pot hydrothermal approach. Morphology and crystal structure of this ternary nanoarchitecture were characterized through scanning electron microscopy, transmission electron microscopy, Raman spectra and X-ray photoelectron spectroscopy. An ultrasensitive non-enzymatic glucose sensor was developed by decorating this ternary nanohybrid on the working electrode of a screen-printed electrochemical sensor. Cycle sweep voltammetry and amperometry were used to study the electro-catalytic activity of the modified working electrode, which demonstrated superior catalytic activity towards glucose oxidation with an extremely low detection limit of 30 nM. Meanwhile, this sensor showed an excellent selectivity in the presence of interfering species such as uric acid, ascorbic acid, etc. Based on the screen-printed technique, enzyme mimic nanomaterials could be easily introduced into portable devices, which opens the way to take non-enzymatic glucose electrochemical sensing towards point-of-care.

Keywords Electrochemical sensor · Non-enzymatic glucose sensing · Ternary electrode · Screen-printed · Electron transfer

1 Introduction

Glucose is an important biological indicator associated with kidney dysfunction, cardiopathy, retinopathy, etc. Therefore, rapid and effective detection of glucose is crucial for the treatment and control of diabetes. Electrochemical sensors have become the most effective tool for glucose sensors because of their attractive features, such as low production cost, simple instrument, easy operation, time efficiency, and excellent sensitivity (Wang 2008; Chen et al. 2013). Even though enzyme-based sensors exhibit sensitivity and selectivity, the activity of enzyme is environmentally sensitive, and easily affected by many factors, such as pH value, humidity and toxic chemicals (Wilson 1992; Qiang et al. 2011).

In recent years, extensive efforts have been made to develop suitable non-enzymatic sensors, and the advantage of a direct electron transfer mechanism for this generation biosensors has attracted tremendous attention (Niu et al. 2013; Hwang et al. 2018). As a single layer of a two-dimensional lattice nanomaterial, graphene forms a vast platform for loading many different particles, providing new pathways for the synthesis of functional nanocomposites with different properties (Muszynski et al. 2008; Shi et al. 2013; Li et al. 2016). With the research fever of graphene, other lamellar-structured transition metal dichalcogenides (TMDs), such as MoS_2 or WS_2, with a sandwich structure of three hexagonal atomic layers, has demonstrated great potential in electrochemical biosensing (Ramakrishna Matte et al. 2010; Wang et al. 2017; Shavanova et al. 2016). Moreover, by combining conductive and chemically inert graphene with electroactive TMDs, has significantly increased the electrode's kinetics and improve the electrocatalytic activity (Yoon et al. 2017; Song et al. 2014). Structural design and tailoring are also important to enhance sensitivity. To date, a group of first-row transition metals (Co, Ni, Cu, etc) doped electrocatalysts has been widely reported which achieves satisfactory electrochemical performance by increasing the specific surface area

Electronic supplementary material The online version of this article (https://doi.org/10.1007/s10544-020-0472-z) contains supplementary material, which is available to authorized users.

✉ Tao Hu
hutao@seu.edu.cn

✉ Zhonghua Ni
nzh2003@seu.edu.cn

[1] School of Mechanical Engineering, and Jiangsu Key Laboratory for Design and Manufacture of Micro–Nano Biomedical Instruments, Southeast University, Nanjing 211189, China

Published online: 15 February 2020

and providing many highly accessible active sites on their surfaces (Huang et al. 2014; Huang et al. 2013; Shu et al. 2018; Hoa et al. 2016).

In order to meet the needs for point-of-care, it is necessary to explore fabrication techniques towards portability, miniaturization and ease for integration. Screen-printing technology has provided just the kind of method to take electrochemical biosensors towards on-site analysis (Hyun et al. 2013; Washe et al. 2013). Screen-printed electrodes could be prepared on many types of substrates, such as paper sheets, plastic films, ceramics and stretch thin films. Typically, a screen-printed electrochemical biosensor comprised there electrodes on the same substrate, including the reference, working and counter electrodes, which largely ensured the accuracy and adaptability of bioanalysis (Yamanaka et al. 2016; Arduini et al. 2016). With the modification with a variety of biological analytes such as enzymes, DNA, antibodies, or other recognition elements on the working electrode, many types of cost-effective and hand-held biosensors have been developed for detecting target molecules and applied in routine health care (Chu et al. 2017; Karuppiah et al. 2014; Mohamed 2016).

In this work, a portable, miniaturized, low cost and ultrasensitive non-enzymatic electrochemical glucose biosensor has been developed by using a disposable screen-printed electrodes. To perform this biosensor, the working electrode was modified with a ternary cobalt oxides functionalized MoS_2/reduced graphene oxide (denoted as Co@MoS_2/rGO) nanocomposite, which was prepared through a scalable one-pot hydrothermal method. Detailed morphological and chemical characterizations of this as-prepared nanocomposite were conducted by using scanning electron microscopy (SEM), energy dispersive x-ray spectroscopy (EDS), transmission electron microscopy (TEM), Raman spectra and X-ray photoelectron spectroscopy (XPS). The cyclic voltammetry and amperometric studies of the Co@MoS_2/rGO nanohybrid based screen-printed biosensor exhibited good conductivity and high catalytic activity towards glucose sensing. More significantly, this sensor performed excellently against anti-interference and anti-poisoned activity with extremely low detection limit. The selectivity, stability and practicability made this enzyme-free biosensor promising in the field of point-of-care (POC) or wearable devices.

2 Material and methods

2.1 Reagents and chemicals

Sulfuric acid (H_2SO_4), potassium permanganate ($KMnO_4$), sodium nitrate ($NaNO_3$), cobalt acetate tetrahydrate ($Co(CH_3COO)_2{\cdot}4H_2O$), sodium dodecyl sulfate ($C_{12}H_{25}SO_4Na$), Sodium hydroxide (NaOH) and absolute ethanol (C_2H_6O) were purchased from Sinopharm group chemical reagent Co., Ltd. Expanded graphite was bought from Nanjing XFnano. Sodium molybdate (Na_2MoO_4) and L-cysteine were bought from Shanghai macklin biochemical Co., Ltd. Nafion solution (5 wt%) was purchased from Alfa Aesar. Uric acid (UA), ascorbic acid (AA) and dopamine hydrochloride (DA) were bought from Sigma. All other chemicals were of guaranteed reagent (GR) level and without any further purification. Deionized water (ultra-pure conductivity of ≥18 MΩ) obtained from a Milli-Q water system was used throughout the experiment.

2.2 Preparation of cobalt doped MoS_2/rGO nanocomposites

The preparation of cobalt doped MoS_2/rGO nanocomposites (Co@MoS_2/rGO) was carried out by a one-pot hydrothermal method. The specific process was as follows. Firstly, 0.1 mmol $Co(CH_3COO)_2{\cdot}4H_2O$ was put into 20 mL deionized water. After being fully dissolved, the mixed solution was added into a 2.5 mg/mL GO suspension. The mixture solution was stirred for 12 h at room temperature to make sure Co^{2+} could be sufficiently attached to GO nanosheets. Then, 1.35 mmol Na_2MoO_4 and 7.5 mmol L-cysteine were added into the mixture solution under stirring. Finally, the above solution was transferred into a Teflon-lined stainless autoclave and kept at 180 °C for 24 h. After cooling down, the product was repeatedly centrifuged and rinsed for five times with deionized water and absolute ethanol, and then dried in an oven at 80 °C for 6 h to obtain Co@MoS_2/rGO. MoS_2/rGO was also synthesized for electrochemical performance comparison. For the preparation of MoS_2/rGO, $Co(CH_3COO)_2{\cdot}4H_2O$ was not added and the other procedures were the same as that of Co@MoS_2/rGO.

2.3 Construction of the modified glassy carbon electrode (GCE)

The pretreatment procedure of GCE was stated in the supplementary materials S1. After that, the proper amount of Co@MoS_2/rGO or MoS_2/rGO was mixed with Nafion solution and absolute ethanol (19:1). Then 8 μL suspension was added dropwise onto the GCE and naturally dried for use.

2.4 Construction of the modified screen-printed electrode (SPE)

Details on the fabrication of SPEs were given in the supplementary materials S2. The screen-printing layers and electrode dimensions were shown in Fig. S1. The quality and properties of different batches of SPEs were characterized with the electrical measurements, including resistance test and cyclic voltammetry technique. After that, proper amount of the as-prepared Co@MoS_2/rGO or MoS_2/rGO suspension was

added dropwise onto the working electrode of SPE and naturally dried for use.

2.5 Instrumentation and measurements

Electrochemical measurements were performed with a CHI 660E electrochemical workstation (Shanghai Chenhua Instrument Co., China) in a conventional three-electrode configuration (NaOH, 0.1 M, 40 mL) by adopting modified GCE (4 mm in diameter) as the working electrode (WE), platinum sheet as the counter electrode (CE) and Ag/AgCl (3 M KCl saturated) as the reference electrode (RE), respectively. For modified SPEs measurement, the electrolyte was 5 mM $K_3[Fe(CN)_6]$ and 0.1 M KCl. Scanning electron microscopy (SEM) images were obtained using an FEI Quanta 200 microscope. Transmission electron microscope (TEM) and energy-dispersive X-ray spectroscopy (EDS) were carried out on an FEI Tecnai G2 T20 microscope operating at 200 kV. Raman spectra, X-ray photoelectron spectroscopy data were acquired using WITec Alpha300R, PHI 5000 VersaProbe, respectively.

3 Results and discussion

3.1 Structural characterization

The schematic illustration for the fabrication and electrochemical tests of the screen-printed biosensor with a ternary non-enzymatic Co@MoS_2/rGO modified working electrode is demonstrated in Fig. 1. The preparation procedure of Co@MoS_2/rGO is described in Section 2.2. The morphology characterization for the graphite working electrode of SPEs is given in Fig. S2.

Figure 2a and b show the morphology of Co@MoS_2/rGO with SEM and TEM techniques, illustrating the three-dimensional (3D) sphere-like architecture, establishing an interconnected conducting network and reducing the charger diffusion resistance, which benefits the efficient electronic transport in electrochemical reactions. Cobalt dopping provided abundant metal active edges, which played a significant role in the reactivity enhancement. To confirm this statement, MoS_2/rGO was prepared by the same method for comparison. Fig. S3 and Fig. S4 show the EDS analysis of Co@MoS_2/rGO and MoS_2/rGO, respectively. The Co, Mo, S, O, and C elements are present in the case of Co@MoS_2/rGO nanocomposites with an atomic ratio of Co:Mo:S:C:O = 0.2:2.6:4.9:3.5:1. And Mo, S, O, and C elements are present in the case of MoS_2/rGO nanocomposites with an atomic ratio of Mo:S:C:O = 4.0:8.6:4.8:1. All of these results confirm the successfully prepared MoS_2/rGO and Co@MoS_2/rGO nanocomposites. Figure 2c shows the Raman spectra of rGO and Co@MoS_2/rGO. The black curve shows the characteristic peaks at 1342 cm^{-1} and 1592 cm^{-1} which are assigned to typical D and G peaks of rGO, and peaks located at 381 cm^{-1} and 407 cm^{-1} confirm the presence of MoS_2 in Co@MoS_2/rGO (Ma et al. 2016).

XPS is adopted to confirm the existence of the cobalt compound and determine the chemical bonding structures in the composite. High-resolution peak differentiation results of Mo (3d) and S (2p) in MoS_2/rGO are plotted in Fig. S5. Figure 2d–f display the detailed XPS scan for Mo (3d), S (2p) and Co (2p) binding energies of Co@MoS_2/rGO, respectively. Two characteristic peaks at 227.8 and 230.9 eV, are assigned to the Mo $3d_{5/2}$ and $3d_{3/2}$ binding energies for Mo^{4+}. The observation of peaks at 229.0 and 232.0 eV suggests the presence of Mo^{5+} ions (Chang et al. 2013; Vrubel et al. 2012). Meanwhile, the peaks, corresponding to the S $2p_{3/2}$ and $2p_{1/2}$ orbitals of divalent sulfide ions (S^{2-}) are observed at 160.6 and 161.9 eV. The stoichiometric ratio (S:Mo) estimated from the respective integrated peak area of XPS spectra is 1.9, indicating that the structure is close to MoS_2. Co 2p spectra reveal two distinct peaks corresponding to Co $2p_{3/2}$ and Co $2p_{1/2}$ at binding energies of 778.4 and 793.9 eV accompanying with two weaker satellite

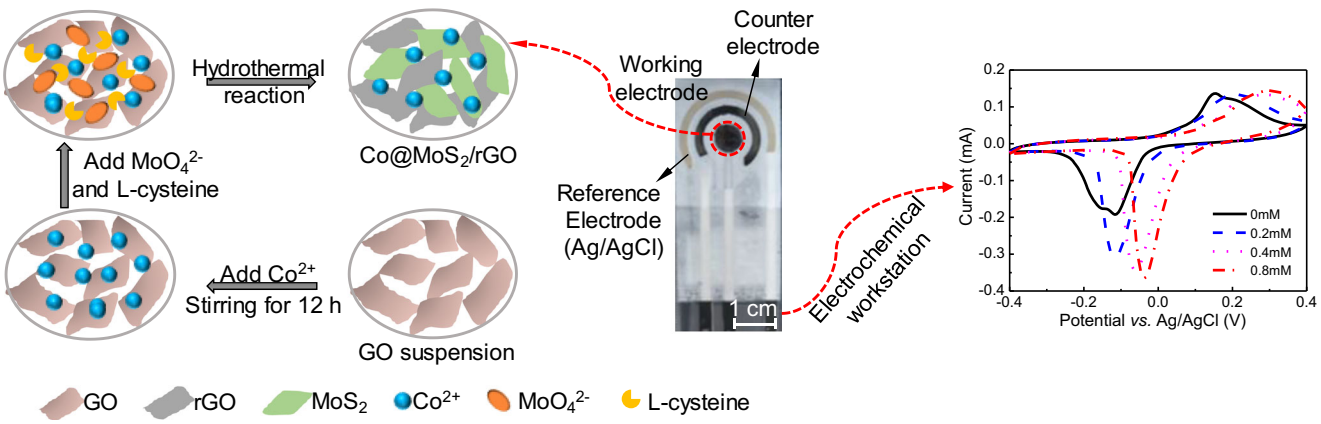

Fig. 1 Schematic illustration for the fabrication and electrochemical tests of the screen-printed biosensor with ternary non-enzymatic Co@MoS_2/rGO modified working electrode

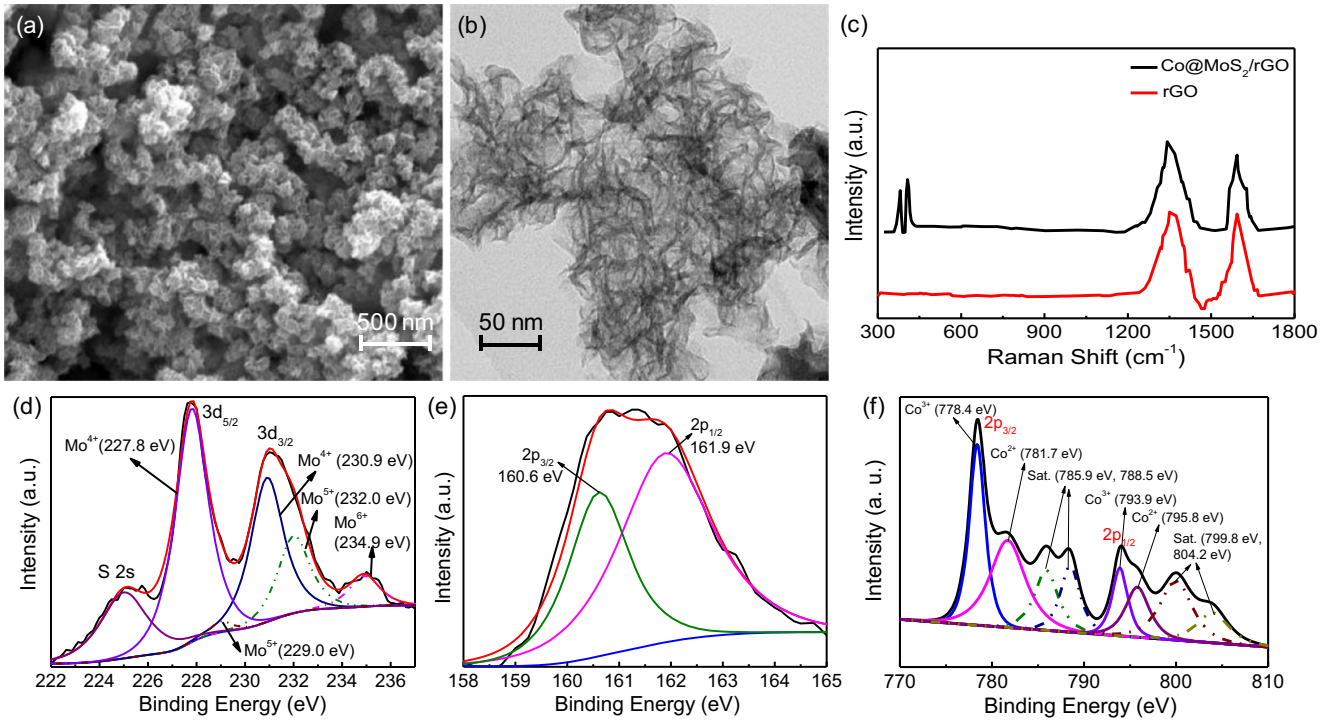

Fig. 2 **a** SEM, and **b** TEM characterization of Co@MoS_2/rGO; **c** Raman spectra of rGO and Co@MoS_2/rGO; **d**–**f** High resolution XPS scan for Mo (3d), S (2p) and Co (2p) binding energies of Co@MoS_2/rGO, respectively

peaks located at 785.9 and 799.8 eV due to spin-energy separation, suggesting the existence of Co^{3+}. Furthermore, the principal peaks can be fitted into four subpeaks, of which the fitting peaks at 781.7 and 795.8 eV with the satellite peaks at 788.5 and 804.2 eV are indexed to Co^{2+} (Xu et al. 2019; Li et al. 2019; Vilian et al. 2018). These results depict the successful dopping of Co_3O_4 structure in this nanohybrid, and the atomic concentration tables of MoS_2/rGO and Co@MoS_2/rGO are provided in Table S1 and Table S2.

3.2 Electrochemical characterization of nanocomposites modified GCE

Electrochemical tests for different working electrodes were performed in a three-electrode cell system. Figure 3a displays the cyclic voltammetry (CV) curves of MoS_2/rGO and Co@MoS_2/rGO modified GCEs in 0.1 M NaOH solution in the absence and presence of 4 mM glucose under a scan rate of 50 mV/s. The current density of both electrodes increases noticeably after 4 mM glucose is added, suggesting their glucose catalytic activity. Moreover, the CV plot of Co@MoS_2/rGO electrode shows a larger current response comparing to that of MoS_2/rGO electrode, suggesting cobalt dopping plays a significant role in glucose sensing. Figure 3b shows the chronocoulometric results on the bare and modified GCEs, which are governed by the following Eq. (1).

$$Q = \left(2n\ \mathrm{F}\ \mathrm{A}\ {D_0}^{1/2}\pi^{-1/2}C_0\right)t^{1/2} \quad (1)$$

Where Q is the absolute value of the reduction charge, n is the number of electrons transferred, F is the Faraday constant, A is the electrode area, t is the time, D_0 and C_0 are the diffusion coefficient and the bulk concentration of the oxidized complex, respectively. Based on this equation, Q is versus $t^{1/2}$ as shown in Fig. 3b, with the slope indicating the electrode kinetics and the adsorption property of electroactive materials (Jeong et al. 2017). The slope of Co@MoS_2/rGO is much larger than that of MoS_2/rGO, elucidating that the ternary hybrid electrode provides more excellent charge transfer ability than MoS_2/rGO.

CV curves of different electrodes measured at scan rates of 10 to100 mV/s are presented in Fig. S6. As shown in Fig. S7, the current density increases almost linearly as a function of scan rate. The specific capacitance of Co@MoS_2/rGO obtained from the slope of the linear fitting is 9.06 mF/cm^2, which is larger than that of MoS_2/rGO (2.52 mF/cm^2), suggesting the ternary electrode possesses better electrochemical capacitive behavior. The CV responses of Co@MoS_2/rGO modified GCE towards different glucose concentrations ranging from 0 to 10 mM are plotted in Fig. 3c and Fig. S8. As expected, the oxidation current density increased continuously with the glucose concentration, especially at 0.65 V (vs. Ag/AgCl). This may be because Co^{2+} is catalytically active during the oxidation of glucose to gluconolactone, based on the reactions shown in Eq. (2)–(4) (Li et al. 2019; Vilian et al. 2018).

$$Co_3O_4 + OH^- + H_2O \rightleftharpoons 3CoOOH + e^- \quad (2)$$

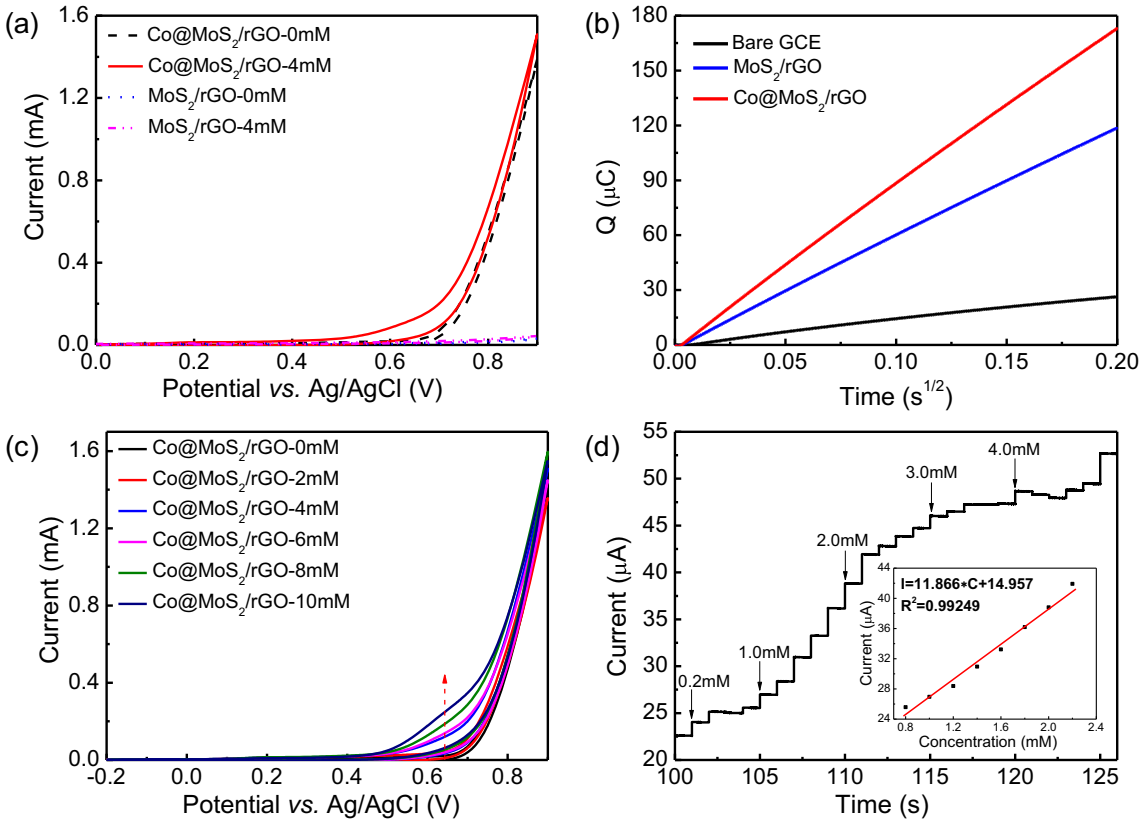

Fig. 3 **a** CV curves of MoS_2/rGO and Co@MoS_2/rGO modified GCEs in 0.1 M NaOH solution in the absence and presence of 4 mM glucose; **b** Chronocoulometric results on the bare GCE, MoS_2/rGO modified GCE and Co@MoS_2/rGO modified GCE; **c** CV responses of Co@MoS_2/rGO modified GCE towards different glucose concentration ranging from 0 to 10 mM; **d** Amperometric responses of the Co@MoS_2/rGO modified GCE after successive addition of glucose at the applied potential of 0.65 V (vs. Ag/AgCl); Inset is a plot of the steady-state current vs. glucose concentration in the linear range up to 2.2 mM

$$CoOOH + OH^- \rightleftharpoons CoO_2 + H_2O + e^- \quad (3)$$

$$2CoO_2 + C_6H_{12}O_6\ (\text{glucose}) \rightleftharpoons 2CoOOH + C_6H_{10}O_6\ (\text{gluconolactone}) \quad (4)$$

To evaluate the linear working range of the Co@MoS_2/rGO modified GCE, the amperometric response was assessed after the successive injection of glucose into 0.1 M NaOH under continuous stirring at an applied potential of 0.65 V (Fig. 3d). After the addition of glucose, the current increases, reaching more than 95% steady-state current is less than 1 s, indicating faster electron communication between glucose and the ternary electrode. From a plot of the steady-state current vs. glucose concentration in the linear range up to 2.2 mM displayed in the inset of Fig. 3d, the obtained linear regression equation is I (uA) = 11.866*C (mM) + 14.957 (R^2 = 0.99249). Based on the slope of this regression, the sensitivity of Co@MoS_2/rGO is calculated to be 131.84 uA mM^{-1} cm^{-2}.

For comparison, the CV responses of the binary MoS_2/rGO electrode towards different glucose concentrations ranging from 0 to 10 mM are provided in Fig. S9. The electrocatalytic currents increase gradually with glucose concentration while the signal was weaker than that of Co@MoS_2/rGO. Herein, MoS_2/rGO exhibited the parallel ability to glucose oxidation with relatively low sensitivity. In the proposed ternary Co_3O_4 functionalized MoS_2/rGO structure, rational incorporation of MoS_2 as an electron collector can largely accelerate the charge transfer. Both the rGO and MoS_2 nanosheets promote the formation of conductive path and inhibit the aggregation of Co_3O_4 nanoparticles. Synergistic effect among these three components contributes to the electrocatalytic performance enhancement, and an extremely low LOD of 30 nM is interpreted (S/N = 3) from inset of Fig. 3d, which could also be confirmed by amperometric test, as shown in Fig. S10. The key performance indicators of the ternary Co@MoS_2/rGO were compared with other transition metal-based enzyme-free catalysts, which was provided in Table S3. Evidently, the as-prepared Co@MoS_2/rGO showed extremely low LOD, suggesting it would be a promising electrode material for electrochemical biosensing.

3.3 Electrochemical characterization of nanocomposites modified SPE

Typical CV curves of bare SPE and Co@MoS_2/rGO modified SPE estimated in 5 mM $K_3[Fe(CN)_6]$ and 0.1 M KCl with a

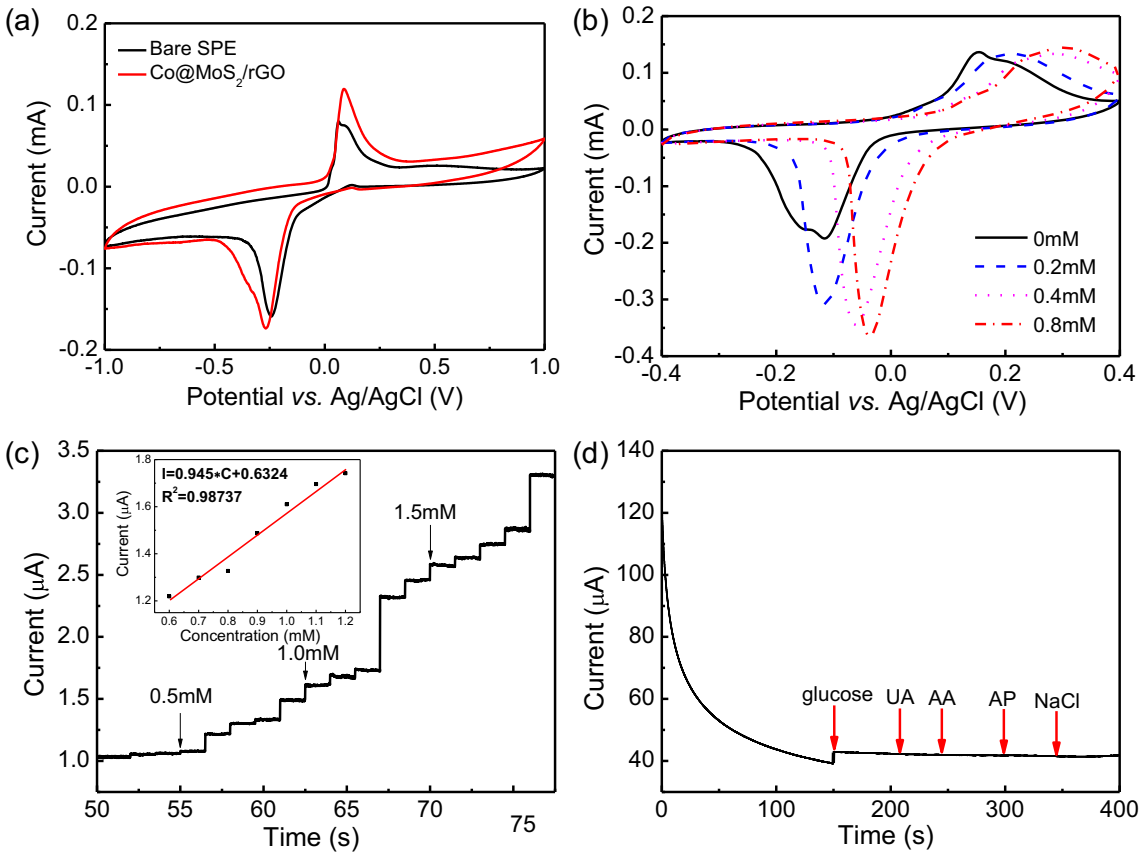

Fig. 4 **a** CV curves of bare SPE and Co@MoS_2/rGO modified SPE; **b** CV responses of Co@MoS_2/rGO modified SPE towards different glucose concentration ranging from 0 to 0.8 mM; **c** Amperometric responses of the Co@MoS_2/rGO modified SPE after successive addition of glucose into potassium ferricyanide electrolyte at the applied potential of 0.15 V (vs. Ag/AgCl); Inset is a plot of the steady-state current vs. glucose concentration in the linear range up to 1.2 mM; **d** Amperometric response curve of Co@MoS_2/rGO modified SPE to the addition of glucose and interfering agents (UA, AA, AP and NaCl)

scan rate of 50 mV/s are shown in Fig. 4a. Co@MoS_2/rGO modified SPE shows a better defined reversible CV curve and higher electrical current, which is attributed to the porous and interconnected conductive network, facilitating ion and electron transport significantly. The CV responses of Co@MoS_2/rGO modified SPE towards different glucose concentrations ranging from 0 to 0.8 mM are plotted in Fig. 4b. Both the anodic and cathodic current density increase continuously with the glucose concentration. The amperometric response was conducted after successive injection of glucose into potassium ferricyanide electrolytes under continuous stirring at an applied potential of 0.15 V to evaluate the linear working range of the Co@MoS_2/rGO modified SPE (Fig. 4c). From a plot of the steady-state current vs. glucose concentration in the linear range up to 1.2 mM displayed in the inset of Fig. 4c, the obtained linear regression equation is I (uA) = 0.945*C (mM) + 0.6324 (R^2 = 0.98737). Compared to Co@MoS_2/rGO modified GCE, the sensitivity was relatively low, probably resulting from the topological structure, position and surface morphology of the SPEs. In the follow-up study, the distribution and dimension of SPEs along with the fabrication and modification procedures should be further optimized.

As one of the most important analytical factors, the anti-interface capability of the proposed non-enzymatic biosensor was assessed by the amperometric test with successive additions of 1.0 mM glucose and 0.2 mM interfaces including uric acid (UA), ascorbic acid (AA), paracetamol and sodium chloride (NaCl) into the electrolyte. The obtained result is shown in Fig. 4d, after the addition of glucose, a clear amperometric response is shown by the modified SPE, while the addition of interference species does not lead to any noticeable amperometric response, demonstrating the superior selectivity of this biosensor.

4 Conclusion

In summary, we have constructed a screen-printed electrochemical biosensor based on a ternary Co@MoS_2/rGO modified working electrode for non-enzymatic glucose sensing.

Co@MoS_2/rGO was synthesized by a facile hydrothermal method, exhibiting a wide linear range, high sensitivity, low detection limit of 30 nM, which was benefited to the synergistic and electrocatalytic effects of the Co_3O_4, MoS_2 and rGO nanosheets. Furthermore, the as-prepared electrode established a large surface area, supporting a large number of electroactive species, which considerably enhanced the charge transfer. All the experimental results indicate Co@MoS_2/rGO nanocomposite is a promising enzyme-free candidate for glucose detection. The convenient modification procedure together with the favorable electrocatalytic performance of this as-fabricated screen-printed biosensor, suggest that Co@MoS_2/rGO modified SPEs hold great potential to the disposable, wearable and mass production of low cost for the non-enzymatic glucose sensing.

Acknowledgments This work was supported by the National Key Scientific Instrument and Equipment Development Project (Grant No.: 51627808), National Natural Science Foundation of China (Grant No. 51605088), Natural Science Foundation of Jiangsu Province (Grant No. BK20170667) and Shuangchuang Talent Project of Jiangsu Province (Grant No. 1102000208).

References

F. Arduini, L. Micheli, D. Moscone, G. Palleschi, S. Piermarini, F. Ricci, G. Volpe, Electrochemical biosensors based on nanomodified screen-printed electrodes: Recent applications in clinical analysis. Trends Anal. Chem. **79**, 114–126 (2016)

Y.H. Chang, C.T. Lin, T.Y. Chen, C.L. Hsu, Y.H. Lee, W. Zhang, K.H. Wei, L.J. Li, Highly efficient electrocatalytic hydrogen production by MoS_x grown on graphene-protected 3D Ni foams. Adv. Mater. **25**, 756–760 (2013)

C. Chen, Q. Xie, D. Yang, H. Xiao, Y. Fu, Y. Tan, S. Yao, Recent advances in electrochemical glucose biosensors: A review. RSC Adv. **3**, 4473–4491 (2013)

Z. Chu, J. Peng, W. Jin, Advanced nanomaterial inks for screen-printed chemical sensors. Sensors Actuators B Chem. **243**, 919–926 (2017)

L.T. Hoa, J.S. Chung, S.H. Hur, A highly sensitive enzyme-free glucose sensor based on Co_3O_4 nanoflowers and 3D graphene oxide hydrogel fabricated via hydrothermal synthesis. Sensors Actuators B Chem. **223**, 76–82 (2016)

J. Huang, Z. Dong, Y. Li, J. Li, W. Tang, H. Yang, J. Wang, Y. Bao, J. Jin, R. Li, MoS_2 nanosheet functionalized with cu nanoparticles and its application for glucose detection. Mater. Res. Bull. **48**, 4544–4547 (2013)

J. Huang, Y. He, J. Jin, Y. Li, Z. Dong, R. Li, A novel glucose sensor based on MoS_2 nanosheet functionalized with Ni nanoparticles. Electrochim. Acta **136**, 41–46 (2014)

D.W. Hwang, S. Lee, M. Seo, T.D. Chung, Recent advances in electrochemical non-enzymatic glucose sensors-a review. Anal. Chim. Acta **1033**, 1–34 (2018)

W.J. Hyun, O.O. Park, B.D. Chin, Foldable graphene electronic circuits based on paper substrates. Adv. Mater. **25**, 4729–4734 (2013)

J.M. Jeong, M. Yang, D.S. Kim, T.J. Lee, B.G. Choi, D.H. Kim, High performance electrochemical glucose sensor based on three-dimensional MoS_2/graphene aerogel. J. Colloid Interface Sci. **506**, 379–385 (2017)

C. Karuppiah, S. Palanisamy, S.M. Chen, V. Veeramani, P. Periakaruppan, Direct electrochemistry of glucose oxidase and sensing glucose using a screen-printed carbon electrode modified with graphite nanosheets and zinc oxide nanoparticles. Microchim. Acta **181**, 1843–1850 (2014)

X. Li, L. Zhang, X.B. Zang, X.M. Li, H.W. Zhu, Photo-promoted platinum nanoparticles decorated MoS_2@graphene woven fabric catalyst for efficient hydrogen generation. ACS Appl. Mater. Interfaces **8**, 10866–10873 (2016)

X. Li, K. Ren, M. Zhang, W. Sang, D. Sun, T. Hu, Z. Ni, Cobalt functionalized MoS_2/carbon nanotubes scaffold for enzyme-free glucose detection with extremely low detection limit. Sensors Actuators B Chem. **293**, 122–128 (2019)

L. Ma, Y. Hu, G. Zhu, R. Chen, T. Chen, H. Lu, Y. Wang, J. Liang, H. Liu, C. Yan, Z. Tie, Z. Jin, J. Liu, In situ thermal synthesis of inlaid ultrathin MoS_2/graphene nanosheets as electrocatalysts for the hydrogen evolution reaction. Chem. Mater. **28**, 5733–5742 (2016)

H.M. Mohamed, Screen-printed disposable electrodes: Pharmaceutical applications and recent developments. Trends Anal. Chem. **82**, 1–11 (2016)

R. Muszynski, B. Seger, P.V. Kamat, In situ synthesis of metal nanoparticles on single-layer graphene oxide and reduced graphene oxide surfaces. J. Phys. Chem. C **112**, 5263–5266 (2008)

X. Niu, M. Lan, H. Zhao, C. Chen, Highly sensitive and selective nonenzymatic detection of glucose using three-dimensional porous nickel nanostructures. Anal. Chem. **85**, 3561–3569 (2013)

L. Qiang, S. Vaddiraju, D. Patel, F. Papadimitrakopoulos, Edge-plane microwire electrodes for highly sensitive H_2O_2 and glucose detection. Biosens. Bioelectron. **26**, 3755–3760 (2011)

H.S.S. Ramakrishna Matte, A. Gomathi, A.K. Manna, D.J. Late, R. Datta, S.K. Pati, C.N.R. Rao, MoS_2 and WS_2 analogues of Graphene. Angew. Chem. Int. Ed. **49**, 4059–4062 (2010)

K. Shavanova, Y. Bakakina, I. Burkova, I. Shtepliuk, R. Viter, A. Ubelis, V. Beni, N. Starodub, R. Yakimova, V. Khranovskyy, Application of 2D non-graphene materials and 2D oxide nanostructures for biosensing technology. Sensors **223**, 1–23 (2016)

X. Shi, H. Gong, Y. Li, Graphene-based magnetic plasmonic nanocomposite for dual bioimaging and photothermal therapy. Biomaterials. **34**, 4786–4793 (2013)

Y. Shu, B. Li, J. Chen, Q. Xu, H. Pang, X. Hu, Facile synthesis of ultrathin nickel−cobalt phosphate 2D nanosheets with enhanced electrocatalytic activity for glucose oxidation. ACS Appl. Mater. Interfaces **10**, 2360–2367 (2018)

H. Song, Y. Ni, S. Kokot, Investigations of an electrochemical platform based on the layered MoS_2-graphene and horseradish peroxidase nanocomposite for direct electrochemistry and electrocatalysis. Biosens. Bioelectron. **56**, 137–143 (2014)

A.T.E. Vilian, B. Dinesh, M. Rethinasabapathy, S.K. Hwang, C.S. Jin, Y.S. Huh, Y.K. Han, Hexagonal Co_3O_4 anchored reduced graphene oxide sheets for high-performance supercapacitors and nonenzymatic glucose sensing. J. Mater. Chem. A **6**, 14367–14379 (2018)

H. Vrubel, D. Merki, X. Hu, Hydrogen evolution catalyzed by MoS_3 and MoS_2 particles. Energy Environ. Sci. **5**, 6136–6144 (2012)

J. Wang, Electrochemical glucose biosensors. Chem. Rev. **108**, 814–825 (2008)

Y.H. Wang, K.J. Huang, X. Wu, Recent advances in transition-metal dichalcogenides based electrochemical biosensors: A review. Biosens. Bioelectron. **97**, 305–316 (2017)

A. Washe, P. Lozano-Sanchez, D. Bejarano-Nosas, Facile and versatile approaches to enhancing electrochemical performance of screen printed electrodes. Electrochim. Acta **91**, 166–172 (2013)

R. Wilson, Glucose oxidase: an ideal enzyme. Biosens. Bioelectron. **7**, 165–185 (1992)

J. Xu, F. Li, D. Wang, M. Hasnain Nawaz, Q. An, D. Han, L. Niu, Co_3O_4 nanostructures on flexible carbon cloth for crystal plane effect of nonenzymatic electrocatalysis for glucose. Biosens. Bioelectron. **123**, 25–29 (2019)

K. Yamanaka, M.C. Vestergaard, E. Tamiya, Printable electrochemical biosensors: A focus on screen-printed electrodes and their application. Sensors **16**, 1761 (2016)

J. Yoon, T. Lee, B. Bapurao G, J. Jo, B.K. Oh, J.W. Choi, Electrochemical H_2O_2 biosensor composed of myoglobin on MoS_2 nanoparticle-graphene oxide hybrid structure. Biosens. Bioelectron. **93**, 14–20 (2017)